Production of $b\bar{b}$ at forward rapidity in p+p collisions at $\sqrt{s} = 510$ GeV

U. Acharya,[20] A. Adare,[11] C. Aidala,[42] N.N. Ajitanand,[60,*] Y. Akiba,[55,56,†] R. Akimoto,[10] M. Alfred,[23] N. Apadula,[28,61] Y. Aramaki,[55] H. Asano,[35,55] E.T. Atomssa,[61] T.C. Awes,[51] B. Azmoun,[7] V. Babintsev,[24] M. Bai,[6] N.S. Bandara,[41] B. Bannier,[61] K.N. Barish,[8] S. Bathe,[5,56] A. Bazilevsky,[7] M. Beaumier,[8] S. Beckman,[11] R. Belmont,[11,42,49] A. Berdnikov,[58] Y. Berdnikov,[58] L. Bichon,[65] D. Black,[8] B. Blankenship,[65] J.S. Bok,[48] V. Borisov,[58] K. Boyle,[56] M.L. Brooks,[38] J. Bryslawskyj,[5,8] H. Buesching,[7] V. Bumazhnov,[24] S. Campbell,[12,28] V. Canoa Roman,[61] C.-H. Chen,[56] C.Y. Chi,[12] M. Chiu,[7] I.J. Choi,[25] J.B. Choi,[30,*] T. Chujo,[64] Z. Citron,[66] M. Connors,[20] M. Csanád,[15] T. Csörgő,[67] A. Datta,[47] M.S. Daugherity,[1] G. David,[7,61] K. DeBlasio,[47] K. Dehmelt,[61] A. Denisov,[24] A. Deshpande,[56,61] E.J. Desmond,[7] L. Ding,[28] A. Dion,[61] J.H. Do,[68] A. Drees,[61] K.A. Drees,[6] J.M. Durham,[38] A. Durum,[24] A. Enokizono,[55,57] H. En'yo,[55] R. Esha,[61] S. Esumi,[64] B. Fadem,[43] W. Fan,[61] N. Feege,[61] D.E. Fields,[47] M. Finger,[9] M. Finger, Jr.,[9] D. Firak,[14] D. Fitzgerald,[42] S.L. Fokin,[34] J.E. Frantz,[50] A. Franz,[7] A.D. Frawley,[19] C. Gal,[61] P. Gallus,[13] P. Garg,[3,61] H. Ge,[61] F. Giordano,[25] A. Glenn,[37] Y. Goto,[55,56] N. Grau,[2] S.V. Greene,[65] M. Grosse Perdekamp,[25] Y. Gu,[60] T. Gunji,[10] H. Guragain,[20] T. Hachiya,[45,55,56] J.S. Haggerty,[7] K.I. Hahn,[17] H. Hamagaki,[10] S.Y. Han,[17,33] J. Hanks,[61] S. Hasegawa,[29] X. He,[20] T.K. Hemmick,[61] J.C. Hill,[28] A. Hodges,[20] R.S. Hollis,[8] K. Homma,[22] B. Hong,[33] T. Hoshino,[22] J. Huang,[7,38] S. Huang,[65] Y. Ikeda,[55] K. Imai,[29] Y. Imazu,[55] M. Inaba,[64] A. Iordanova,[8] D. Isenhower,[1] D. Ivanishchev,[53] B.V. Jacak,[61] S.J. Jeon,[44] M. Jezghani,[20] Z. Ji,[61] J. Jia,[7,60] X. Jiang,[38] B.M. Johnson,[7,20] E. Joo,[33] K.S. Joo,[44] D. Jouan,[52] D.S. Jumper,[25] J.H. Kang,[68] J.S. Kang,[21] D. Kawall,[41] A.V. Kazantsev,[34] J.A. Key,[47] V. Khachatryan,[61] A. Khanzadeev,[53] A. Khatiwada,[38] K. Kihara,[64] C. Kim,[33] D.H. Kim,[17] D.J. Kim,[31] E.-J. Kim,[30] H.-J. Kim,[68] M. Kim,[59] Y.K. Kim,[21] D. Kincses,[15] E. Kistenev,[7] J. Klatsky,[19] D. Kleinjan,[8] P. Kline,[61] T. Koblesky,[11] M. Kofarago,[15,67] J. Koster,[56] D. Kotov,[53,58] B. Kurgyis,[15] K. Kurita,[57] M. Kurosawa,[55,56] Y. Kwon,[68] R. Lacey,[60] J.G. Lajoie,[28] D. Larionova,[58] M. Larionova,[58] A. Lebedev,[28] K.B. Lee,[38] S.H. Lee,[28,61] M.J. Leitch,[38] M. Leitgab,[25] N.A. Lewis,[42] X. Li,[38] S.H. Lim,[11,54,68] M.X. Liu,[38] S. Lökös,[15] D. Lynch,[7] T. Majoros,[14] Y.I. Makdisi,[6] M. Makek,[66,69] A. Manion,[61] V.I. Manko,[34] E. Mannel,[7] M. McCumber,[38] P.L. McGaughey,[38] D. McGlinchey,[11,38] C. McKinney,[25] A. Meles,[48] M. Mendoza,[8] B. Meredith,[12] W.J. Metzger,[16] Y. Miake,[64] A.C. Mignerey,[40] A.J. Miller,[1] A. Milov,[66] D.K. Mishra,[4] J.T. Mitchell,[7] Iu. Mitrankov,[58] S. Miyasaka,[55,63] S. Mizuno,[55,64] P. Montuenga,[25] T. Moon,[33,68] D.P. Morrison,[7] S.I. Morrow,[65] T.V. Moukhanova,[34] B. Mulilo,[33,55] T. Murakami,[35,55] J. Murata,[55,57] A. Mwai,[60] S. Nagamiya,[32,55] J.L. Nagle,[11] M.I. Nagy,[15] I. Nakagawa,[55,56] H. Nakagomi,[55,64] K. Nakano,[55,63] C. Nattrass,[62] S. Nelson,[18] P.K. Netrakanti,[4] M. Nihashi,[22,55] T. Niida,[64] R. Nouicer,[7,56] N. Novitzky,[31,61,64] A.S. Nyanin,[34] E. O'Brien,[7] C.A. Ogilvie,[28] J.D. Orjuela Koop,[11] J.D. Osborn,[42,51] A. Oskarsson,[39] K. Ozawa,[32,64] R. Pak,[7] V. Pantuev,[26] V. Papavassiliou,[48] S. Park,[59,61] S.F. Pate,[48] L. Patel,[20] M. Patel,[28] J.-C. Peng,[25] W. Peng,[65] D.V. Perepelitsa,[7,11,12] G.D.N. Perera,[48] D.Yu. Peressounko,[34] C.E. PerezLara,[61] J. Perry,[28] R. Petti,[7,61] C. Pinkenburg,[7] R. Pinson,[1] R.P. Pisani,[7] M. Potekhin,[7] A. Pun,[48,50] M.L. Purschke,[7] P.V. Radzevich,[58] J. Rak,[31] N. Ramasubramanian,[61] I. Ravinovich,[66] K.F. Read,[51,62] D. Reynolds,[60] V. Riabov,[46,53] Y. Riabov,[53,58] D. Richford,[5] T. Rinn,[25,28] N. Riveli,[50] D. Roach,[65] S.D. Rolnick,[8] M. Rosati,[28] Z. Rowan,[5] J.G. Rubin,[42] J. Runchey,[28] N. Saito,[32] T. Sakaguchi,[7] H. Sako,[29] V. Samsonov,[46,53] M. Sarsour,[20] S. Sato,[29] S. Sawada,[32] B. Schaefer,[65] B.K. Schmoll,[62] K. Sedgwick,[8] J. Seele,[56] R. Seidl,[55,56] A. Sen,[28,62] R. Seto,[8] P. Sett,[4] A. Sexton,[40] D. Sharma,[61] I. Shein,[24] T.-A. Shibata,[55,63] K. Shigaki,[22] M. Shimomura,[28,45] P. Shukla,[4] A. Sickles,[7,25] C.L. Silva,[38] D. Silvermyr,[39,51] B.K. Singh,[3] C.P. Singh,[3] V. Singh,[3] M. Slunečka,[9] K.L. Smith,[19] R.A. Soltz,[37] W.E. Sondheim,[38] S.P. Sorensen,[62] I.V. Sourikova,[7] P.W. Stankus,[51] M. Stepanov,[41,*] S.P. Stoll,[7] T. Sugitate,[22] A. Sukhanov,[7] T. Sumita,[55] J. Sun,[61] X. Sun,[20] Z. Sun,[14] J. Sziklai,[67] A. Takahara,[10] A. Taketani,[55,56] K. Tanida,[29,56,59] M.J. Tannenbaum,[7] S. Tarafdar,[65,66] A. Taranenko,[46,60] A. Timilsina,[28] T. Todoroki,[55,56,64] M. Tomášek,[13] H. Torii,[10] M. Towell,[1] R. Towell,[1] R.S. Towell,[1] I. Tserruya,[66] Y. Ueda,[22] B. Ujvari,[14] H.W. van Hecke,[38] M. Vargyas,[15,67] J. Velkovska,[65] M. Virius,[13] V. Vrba,[13,27] E. Vznuzdaev,[53] X.R. Wang,[48,56] D. Watanabe,[22] Y. Watanabe,[55,56] Y.S. Watanabe,[10,32] F. Wei,[48] S. Whitaker,[28] S. Wolin,[25] C.P. Wong,[20,38] C.L. Woody,[7] Y. Wu,[8] M. Wysocki,[51] B. Xia,[50] Q. Xu,[65] L. Xue,[20] S. Yalcin,[61] Y.L. Yamaguchi,[10,61] A. Yanovich,[24] I. Yoon,[59] I. Younus,[36] I.E. Yushmanov,[34] W.A. Zajc,[12] A. Zelenski,[6] Y. Zhai,[28] S. Zharko,[58] and L. Zou[8]

(PHENIX Collaboration)

[1] *Abilene Christian University, Abilene, Texas 79699, USA*

[2] *Department of Physics, Augustana University, Sioux Falls, South Dakota 57197, USA*

[3] *Department of Physics, Banaras Hindu University, Varanasi 221005, India*

[4] *Bhabha Atomic Research Centre, Bombay 400 085, India*

[5] *Baruch College, City University of New York, New York, New York, 10010 USA*

[6] *Collider-Accelerator Department, Brookhaven National Laboratory, Upton, New York 11973-5000, USA*
[7] *Physics Department, Brookhaven National Laboratory, Upton, New York 11973-5000, USA*
[8] *University of California-Riverside, Riverside, California 92521, USA*
[9] *Charles University, Ovocný trh 5, Praha 1, 116 36, Prague, Czech Republic*
[10] *Center for Nuclear Study, Graduate School of Science, University of Tokyo, 7-3-1 Hongo, Bunkyo, Tokyo 113-0033, Japan*
[11] *University of Colorado, Boulder, Colorado 80309, USA*
[12] *Columbia University, New York, New York 10027 and Nevis Laboratories, Irvington, New York 10533, USA*
[13] *Czech Technical University, Zikova 4, 166 36 Prague 6, Czech Republic*
[14] *Debrecen University, H-4010 Debrecen, Egyetem tér 1, Hungary*
[15] *ELTE, Eötvös Loránd University, H-1117 Budapest, Pázmány P. s. 1/A, Hungary*
[16] *Eszterházy Károly University, Károly Róbert Campus, H-3200 Gyöngyös, Mátrai út 36, Hungary*
[17] *Ewha Womans University, Seoul 120-750, Korea*
[18] *Florida A&M University, Tallahassee, FL 32307, USA*
[19] *Florida State University, Tallahassee, Florida 32306, USA*
[20] *Georgia State University, Atlanta, Georgia 30303, USA*
[21] *Hanyang University, Seoul 133-792, Korea*
[22] *Hiroshima University, Kagamiyama, Higashi-Hiroshima 739-8526, Japan*
[23] *Department of Physics and Astronomy, Howard University, Washington, DC 20059, USA*
[24] *IHEP Protvino, State Research Center of Russian Federation, Institute for High Energy Physics, Protvino, 142281, Russia*
[25] *University of Illinois at Urbana-Champaign, Urbana, Illinois 61801, USA*
[26] *Institute for Nuclear Research of the Russian Academy of Sciences, prospekt 60-letiya Oktyabrya 7a, Moscow 117312, Russia*
[27] *Institute of Physics, Academy of Sciences of the Czech Republic, Na Slovance 2, 182 21 Prague 8, Czech Republic*
[28] *Iowa State University, Ames, Iowa 50011, USA*
[29] *Advanced Science Research Center, Japan Atomic Energy Agency, 2-4 Shirakata Shirane, Tokai-mura, Naka-gun, Ibaraki-ken 319-1195, Japan*
[30] *Jeonbuk National University, Jeonju, 54896, Korea*
[31] *Helsinki Institute of Physics and University of Jyväskylä, P.O.Box 35, FI-40014 Jyväskylä, Finland*
[32] *KEK, High Energy Accelerator Research Organization, Tsukuba, Ibaraki 305-0801, Japan*
[33] *Korea University, Seoul 02841, Korea*
[34] *National Research Center "Kurchatov Institute", Moscow, 123098 Russia*
[35] *Kyoto University, Kyoto 606-8502, Japan*
[36] *Physics Department, Lahore University of Management Sciences, Lahore 54792, Pakistan*
[37] *Lawrence Livermore National Laboratory, Livermore, California 94550, USA*
[38] *Los Alamos National Laboratory, Los Alamos, New Mexico 87545, USA*
[39] *Department of Physics, Lund University, Box 118, SE-221 00 Lund, Sweden*
[40] *University of Maryland, College Park, Maryland 20742, USA*
[41] *Department of Physics, University of Massachusetts, Amherst, Massachusetts 01003-9337, USA*
[42] *Department of Physics, University of Michigan, Ann Arbor, Michigan 48109-1040, USA*
[43] *Muhlenberg College, Allentown, Pennsylvania 18104-5586, USA*
[44] *Myongji University, Yongin, Kyonggido 449-728, Korea*
[45] *Nara Women's University, Kita-uoya Nishi-machi Nara 630-8506, Japan*
[46] *National Research Nuclear University, MEPhI, Moscow Engineering Physics Institute, Moscow, 115409, Russia*
[47] *University of New Mexico, Albuquerque, New Mexico 87131, USA*
[48] *New Mexico State University, Las Cruces, New Mexico 88003, USA*
[49] *Physics and Astronomy Department, University of North Carolina at Greensboro, Greensboro, North Carolina 27412, USA*
[50] *Department of Physics and Astronomy, Ohio University, Athens, Ohio 45701, USA*
[51] *Oak Ridge National Laboratory, Oak Ridge, Tennessee 37831, USA*
[52] *IPN-Orsay, Univ. Paris-Sud, CNRS/IN2P3, Université Paris-Saclay, BP1, F-91406, Orsay, France*
[53] *PNPI, Petersburg Nuclear Physics Institute, Gatchina, Leningrad region, 188300, Russia*
[54] *Pusan National University, Pusan 46241, Korea*
[55] *RIKEN Nishina Center for Accelerator-Based Science, Wako, Saitama 351-0198, Japan*
[56] *RIKEN BNL Research Center, Brookhaven National Laboratory, Upton, New York 11973-5000, USA*
[57] *Physics Department, Rikkyo University, 3-34-1 Nishi-Ikebukuro, Toshima, Tokyo 171-8501, Japan*
[58] *Saint Petersburg State Polytechnic University, St. Petersburg, 195251 Russia*
[59] *Department of Physics and Astronomy, Seoul National University, Seoul 151-742, Korea*
[60] *Chemistry Department, Stony Brook University, SUNY, Stony Brook, New York 11794-3400, USA*
[61] *Department of Physics and Astronomy, Stony Brook University, SUNY, Stony Brook, New York 11794-3800, USA*
[62] *University of Tennessee, Knoxville, Tennessee 37996, USA*
[63] *Department of Physics, Tokyo Institute of Technology, Oh-okayama, Meguro, Tokyo 152-8551, Japan*
[64] *Tomonaga Center for the History of the Universe, University of Tsukuba, Tsukuba, Ibaraki 305, Japan*
[65] *Vanderbilt University, Nashville, Tennessee 37235, USA*
[66] *Weizmann Institute, Rehovot 76100, Israel*
[67] *Institute for Particle and Nuclear Physics, Wigner Research Centre for Physics, Hungarian Academy of Sciences (Wigner RCP, RMKI) H-1525 Budapest 114, POBox 49, Budapest, Hungary*

[68] *Yonsei University, IPAP, Seoul 120-749, Korea*
[69] *Department of Physics, Faculty of Science, University of Zagreb, Bijenička c. 32 HR-10002 Zagreb, Croatia*
(Dated: October 28, 2020)

The cross section of bottom quark-antiquark ($b\bar{b}$) production in p+p collisions at $\sqrt{s}$ = 510 GeV is measured with the PHENIX detector at the Relativistic Heavy Ion Collider. The results are based on the yield of high mass, like-sign muon pairs measured within the PHENIX muon arm acceptance ($1.2 < |y| < 2.2$). The $b\bar{b}$ signal is extracted from like-sign dimuons by utilizing the unique properties of neutral B meson oscillation. We report a differential cross section of $d\sigma_{b\bar{b}\to\mu^\pm\mu^\pm}/dy = 0.16 \pm 0.01$ (stat) ± 0.02 (syst) ± 0.02 (global) nb for like-sign muons in the rapidity and p_T ranges $1.2 < |y| < 2.2$ and $p_T > 1$ GeV/c, and dimuon mass of 5–10 GeV/c^2. The extrapolated total cross section at this energy for $b\bar{b}$ production is 13.1 ± 0.6 (stat) ± 1.5 (syst) ± 2.7 (global) μb. The total cross section is compared to a perturbative quantum chromodynamics calculation and is consistent within uncertainties. The azimuthal opening angle between muon pairs from $b\bar{b}$ decays and their p_T distributions are compared to distributions generated using PS PYTHIA6, which includes next-to-leading order processes. The azimuthal correlations and pair p_T distribution are not very well described by PYTHIA calculations, but are still consistent within uncertainties. Flavor creation and flavor excitation subprocesses are favored over gluon splitting.

I. INTRODUCTION

The bottom-quark production in hadron-hadron collisions is an important test of perturbative quantum chromodynamics (pQCD) calculations. Because of its large mass, $m_b \gg \Lambda_{QCD}$, the b-quark production cross section can be reliably calculated by including next-to-leading order (NLO) processes, especially at high center of mass energies [1]. The measurement of the $b\bar{b}$ production cross section over a wide range of colliding energies in hadron-hadron collisions provides a meaningful test of pQCD theory calculations and a baseline measurement for studying modifications of heavy quark production in heavy ion collisions.

Cross section measurements for bottom production in hadron-hadron collision experiments have been made from lower energy fixed-target experiments [2–4] ($\sqrt{s} <$ 45 GeV) up to collider energies ($\sqrt{s} > 100$ GeV). It was found that pQCD predictions match experimental results well at energies greater than $\sqrt{s} = 1$ TeV [5–12], but less so at lower energies. Results at the wide range of collision energies of the Relativistic Heavy Ion Collider explore an important gap between the low-energy fixed-target and TeV-energy regimes.

Without displaced vertex b-tagging capability at PHENIX, b-quark production has been studied using unlike-sign dileptons from heavy quark decays [13]. The PHENIX and STAR collaborations have previously measured the bottom cross section in p+p collisions at $\sqrt{s} =$ 200 GeV using electron-hadron correlations [14, 15] and using dilepton invariant mass and momentum distributions [16–18].

Like-sign dimuons have previously been used to investigate the phenomenon of neutral B meson oscillations in e^+e^- collisions by the CLEO Collaboration [19], the ARGUS Collaboration [20], the ALEPH Collaboration [21], and in $p + \bar{p}$ collisions by the UA1 Collaboration [22]. In this measurement, we use the yield of like-sign dimuons along with the properties of neutral B meson oscillation to determine the $b\bar{b}$ cross section. The correlated like-sign pairs at high mass (5–10 GeV/c^2) are dominated by the semileptonic decay of open bottom pairs and the other correlated sources (i.e. dijets or punch-through hadrons) amount to less than 10%, and therefore provide a clean probe to study the $b\bar{b}$ production.

In the Standard Model, neutral B meson oscillation is a result of higher order weak interactions that transform a neutral B meson into its antiparticle: $B^0 \to \bar{B}^0$ because the flavor eigenstates differ from the physical mass eigenstates of the meson-antimeson system [23, 24]. In the absence of oscillation as shown in Fig. 1(a), primary-primary decays, where the lepton's direct parent is the B meson, can only produce unlike-sign lepton pairs. For example $b \to \bar{B}(B^-, \bar{B}^0, \bar{B}^0_s, ..) \to l^-$ and $\bar{b} \to B(B^+, B^0, B^0_s, ..) \to l^+$ while like-sign lepton pairs can result from a mixture of primary and secondary decays (decay chain).

However, if oscillation occurs, as is the case for neutral B mesons (B^0_d and B^0_s), the $\bar{B}^0$ meson can spontaneously change into a B^0 meson as shown in Fig. 1(b). Unless otherwise noted, we denote $B(\bar{B})$ as a generic admixture of bottom (antibottom) hadrons with production ratios, from weak decays (*i.e.* $Z \to b\bar{b}$) of: $B^+(B^-) = 40.4 \pm 0.9\%$, $B^0(\bar{B}^0) = 40.4 \pm 0.9\%$, $B^0_s(\bar{B}^0_s) = 10.3 \pm 0.9\%$, and $b(\bar{b})$-baryon $= 8.9 \pm 1.5\%$ [25]. The B_c production ratio is negligible (0.2%) and less than the uncertainties associated with bottom hadrons listed above. The time-integrated probability for a neutral B meson to oscillate before it decays is defined as

$$\chi_{d/s} = \frac{1}{2}\frac{(\Delta m/\Gamma)^2}{1 + (\Delta m/\Gamma)^2}\ , \tag{1}$$

where Δm is the mass difference between heavy and light mass eigenstates and Γ is the decay rate of the weak eigenstates. These values are found to be $\chi_d \approx 0.1874 \pm 0.0018$ and $\chi_s \approx 0.499311 \pm 0.000007$ for the B^0_d and B^0_s

* Deceased
† PHENIX Spokesperson: akiba@rcf.rhic.bnl.gov

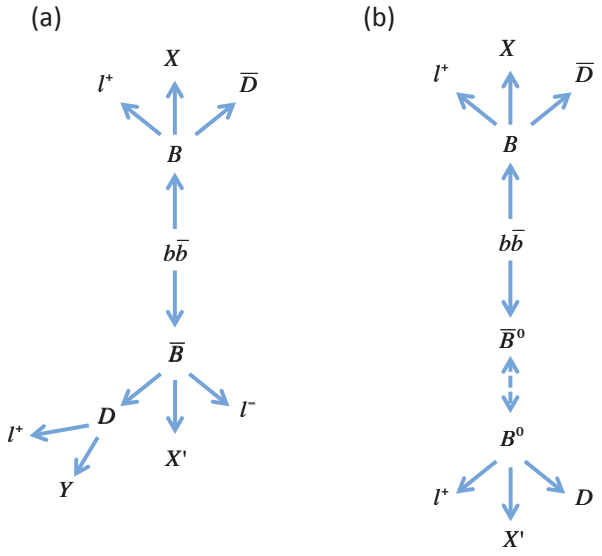

FIG. 1. Example diagrams of lepton pair sources. (a) Like-sign primary-secondary or unlike-sign primary-primary dileptons from B decay chain. (b) Primary-primary dileptons from neutral B meson oscillation.

mesons, respectively [25]. This process can result in a like-sign dilepton event from a primary-primary decay as sown in Fig. 1(b). Given the large branching ratio of the $B \to \mu$ decay channel ($\approx 10.99\%$) [25], the like-sign dilepton from a primary-primary decay provides a unique opportunity for extracting the $b\bar{b}$ cross section.

In this paper, we present measurements of $b\bar{b}$ production cross section through the like-sign dimuon decays and the azimuthal opening angle between the muon pair and their p_T distributions in p+p collisions at $\sqrt{s}$ = 510 GeV at forward ($1.2 < y < 2.2$) and backward ($-2.2 < y < -1.2$) rapidities. The azimuthal opening angle and pair p_T distributions are compared to distributions generated using PYTHIA6 with parton-shower (PS) model [26]. The model approximates the correction to all higher orders (almost next-to-leading-log) for $b\bar{b}$ production, which includes flavor creation, flavor excitation, and gluon splitting. The extrapolated total cross section, using PS PYTHIA6 [26] and PYTHIA8 [27], and MC@NLO [28] calculations, is also presented and compared to pQCD calculation.

The paper is organized as follows: The PHENIX apparatus is described in Sec. II. The data samples used for this analysis and the analysis procedure are presented in Sec. III. The results are presented and discussed in Sec. IV. The summary and conclusions are presented in Sec. V

II. EXPERIMENTAL SETUP

A complete description of the PHENIX detector can be found in Ref. [29]. We briefly describe here only the

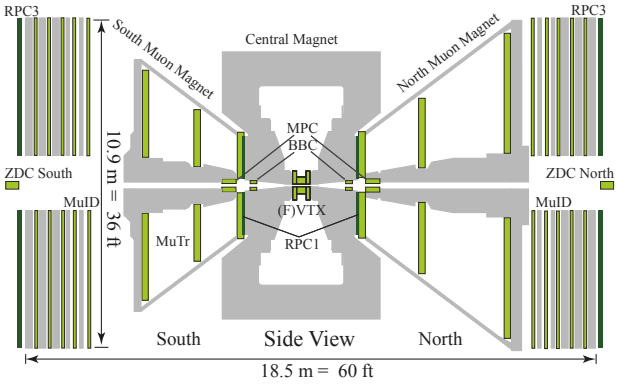

FIG. 2. A side view of the PHENIX detector, concentrating on the muon arm instrumentation.

detector subsystems used in these measurements. The relevant systems, which are shown in Fig. 2, include the PHENIX muon spectrometers covering forward and backward rapidities and the full azimuth. Each muon spectrometer comprises a hadronic absorber, a magnet, a muon tracker (MuTr), and a muon identifier (MuID). The absorbers comprise layers of copper, iron, and stainless steel and have about 7.2 interactions lengths. Following the absorber in each muon arm is the MuTr, which comprises three stations of cathode strip chambers in a radial magnetic field with an integrated bending power of 0.8 T·m. The MuID comprises five alternating steel absorbers and Iarocci tubes. The composite momentum resolution, $\delta p/p$, of particles in the analyzed momentum range is about 5%, independent of momentum and dominated by multiple scattering. Muon candidates are identified by reconstructed tracks in the muon spectrometers.

Another detector system relevant to this analysis is the beam-beam counter (BBC), consisting of two arrays of 64 Čerenkov counters, located on both sides of the interaction point and covering the pseudorapidity range $3.1 < |\eta| < 3.9$. The BBC system was used to measure the p+p collision vertex position along the beam axis ($z_{\rm vtx}$), with 2 cm resolution, and initial collision time. It was also used to measure the beam luminosity and form a minimum bias trigger (MB). The MB trigger requires at least one hit in each BBC on the sides of the interaction point.

III. DATA ANALYSIS

A. Data set and quality cuts

The data set for this analysis is collected by PHENIX during the 2013 p+p run at $\sqrt{s}$ = 510 GeV. Events, in coincidence with the MB trigger, containing a muon pair within the acceptance of the spectrometer are selected by the level-1 dimuon trigger (MuIDLL1-2D) requiring that at least two tracks penetrate through the MuID to

its last two layers. After applying a vertex cut of $|z_{\rm vtx}| < 30$ cm and extensive quality assurance checks, the data remaining correspond to 3.02×10^{12} MB events or to an integrated luminosity of 94.4 pb^{-1}.

A set of cuts was used to select good muon candidates and improve the signal-to-background ratio. Hits in the MuTr are used to make MuTr tracks and hits in the MuID are used to make MuID roads. The MuTr track is required to have more than 9 hits out of the maximum possible of 16 while the MuID road is required to have more than 6 hits out of the maximum possible of 10. Additional χ^2 cut is applied on MuTr track that is calculated from the difference between the measured hit positions of the track and the subsequent fit. MuTr tracks are then projected to the MuID at the first MuID gap and matched to MuID roads by applying cuts on maximum position and angle differences.

Muon candidates are required to have a minimum p_T greater than 1 GeV/c. This cut improves the sample quality by reducing background from pions and kaons. A minimum of 3.0 GeV/c is applied to single muon momentum along the beam axis, p_z, which is reconstructed and energy-loss corrected at the collision vertex, corresponding to the momentum cut effectively imposed by the absorbers. Muon candidates are further restricted to the rapidity range of $-2.2 < y < -1.2$ for the south muon arm and $1.2 < y < 2.2$ for the north muon arm. Additionally, a cut on the χ^2 of the fit of the two muon tracks to the common vertex of the two candidate tracks near the interaction point is applied.

B. Detector acceptance and reconstruction efficiency

The product of the acceptance and reconstruction efficiency ($A\epsilon$) is determined using Monte Carlo (MC) simulation. The $A\epsilon$ is defined by the number of dimuons reconstructed in the muon spectrometers with respect to the number of dimuons generated in the same kinematic region. The kinematic distributions of PYTHIA[1] [30] generated p_T, rapidity, and $b\bar{b}$ mass shape were used as input into a full PHENIX GEANT4 simulation [31].

The p_T and rapidity distributions were tuned such that the reconstructed distributions match those of 2013 data. Variations within the uncertainties of data are taken as systematic uncertainty.

The detector response in the simulation is tuned to a set of characteristics (dead and hot channel maps, gains, noise, etc.) that describes the performance of each detector subsystem. The simulated vertex distribution is also tuned to match that of the 2013 data. The simulated events are further embedded with real data to account for the effects of detector noise and other background tracks, and then are reconstructed in the same manner as the real data. A final cross check was done on J/ψ invariant yield after $A\epsilon$ correction, which matched very well within statistical uncertainties in all p_T and rapidity bins [32].

Figure 3 shows the $A\epsilon$ as a function of (a) dimuon mass $m_{\mu\mu}$, (b) dimuon opening angle $\delta\Phi$, and (c) dimuon p_T. The relative difference in $A\epsilon$ between the two spectrometers is due to different detection efficiencies of the MuTr and MuID systems and different amounts of absorber material.

C. Raw yield extraction

We measure like-sign dimuons in the same muon arm that have an invariant mass between 5 and 10 GeV/c^2. In this mass range, the correlated pairs in the dimuon spectrum are dominated by the semileptonic decay of open bottom pairs either from the primary-secondary decay chain as shown in Fig. 1(a) or from the primary-primary pairs from neutral B meson oscillation as shown in Fig. 1(b). Dileptons from the Drell-Yan process and quarkonia decays can only yield unlike-sign pairs. D mesons can produce like-sign pairs through their decay chain. For example, $c \to D^+ \to \mu^+ + anything$ and the other open charm decays as $\bar{c} \to D^- \to K^+ + anything \to \mu^+\nu_\mu$. However, in the mass range of interest the like-sign pairs from D mesons are negligible. The contribution from neutral D meson oscillation to the like-sign signal is expected to be very small because the oscillation probability is $\mathcal{O}(< 10^{-2})$ [33]; therefore, it is not included.

1. *Correlated background*

Additional contribution to the correlated pairs could originate from correlated sources such as dijets or punch-through hadrons. Hadrons (particularly $\pi^\pm$ and $K^\pm$) can punch through to the last gap of the MuID or decay to muons creating a background to the correlated like-sign signal. These contributions are estimated using MC simulation by determining the p_T-dependent survival probability that a hadron will traverse the muon arm detectors and applying it to PYTHIA generated dihadron pairs to get the yield expected at the back of the muon arm detectors. $\pi^\pm$ and $K^\pm$ are generated with PYTHIA[2] [18, 30, 34] and then run through the PHENIX detector simulation

[1] We used PYTHIA6 (ver 6.421), with parton distribution functions given by CTEQ6LL. The following parameters were modified: MSEL = 0, MSUB(86) = 1, PARP(91) = 2.1, MSTP(51) = 10041, MDME(858,1) = 0, MDME(859,1) = 1, MDME(860,1) = 0, and Tune A.

[2] Non-default parameters used in Multiparton Interaction (MPI)"Tune-A" PS PYTHIA6 simulation for hadron and jet production. The following parameters were modified:MSEL = 1, PMAS(5,1) = 4.1, PYTUNE 100, and PARP(90) = 0.25

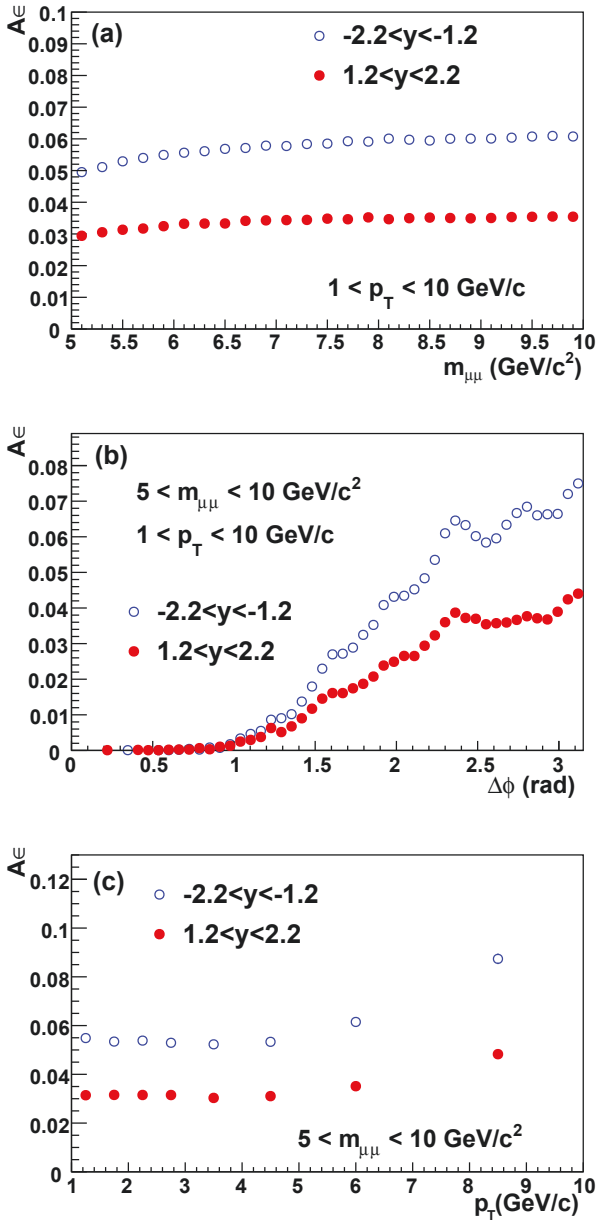

FIG. 3. $A\epsilon$ as a function of (a) invariant mass for like-sign dimuons, (b) dimuon azimuthal opening angle, and (c) dimuon p_T. Shown are the weighted averages of $\mu^+\mu^+$ and $\mu^-\mu^-$ distributions.

chain to determine a p_T-dependent probability that the hadrons penetrate the last gap of the MuID.

To get a better estimate of the survival probability, the hadron simulation is run using two different hadron interaction packages for GEANT: FLUKA and GEISHA [35, 36]. Figure 4 shows the simulated invariant mass spectra from irreducible background are fitted with an exponential function of the form $\exp(a + b \times m + c \times m^2)$ between 5 and 10 GeV/c^2, where m is the invariant mass and a, b and c are fit parameters. The average of the indicated

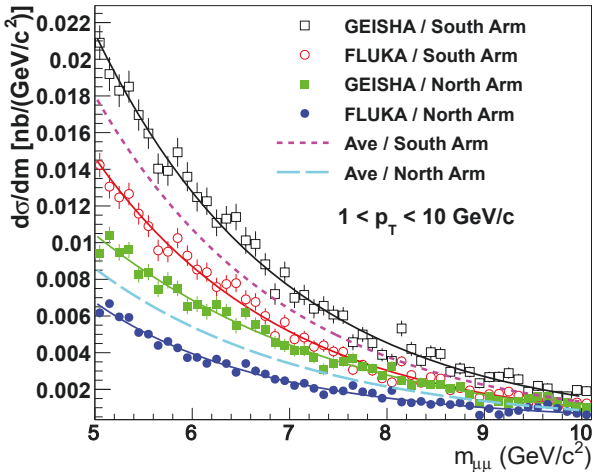

FIG. 4. Like-sign invariant mass distribution from jet background simulation in the north and south arms. The solid lines are fits to the data with an exponential function between 5 and 10 GeV/c^2 while the dashed lines represent the averages of the resulting fits.

results from GEISHA and FLUKA is used to subtract the hadronic background from like-sign pairs while the difference is considered as a systematic uncertainty.

The invariant mass distribution for like-sign pairs is then constructed from PYTHIA generated dihadron pairs within the same event and from mixed events, with each entry weighted by the survival probability. Event-mixing procedure is discussed in the next section. Just as with data, the correlated like-sign signal is obtained by subtracting the mixed event spectrum from the like-sign spectrum, providing the correlated like-sign signal due to dijets or punch-through hadrons. The sum of π and K correlated like-sign signals is weighted based on their p_T-dependent cross sections [37, 38].

Fake like-sign pairs due to charge misidentification and like-sign pairs from Drell-Yan process or quarkonia decays and muon-decayed or punch-through hadrons were also studied and found to be negligible.

2. *Uncorrelated background*

The uncorrelated pair contribution is estimated using event mixing technique [39], where like-sign pairs are constructed by pairing muons in the current event with those of the same sign and same arm in previous events of z-vertex position within 2 cm. The mixed event pairs (N^{BG}_{++} and N^{BG}_{--}) form the uncorrelated background spectrum which is normalized to the the foreground (N^{FG}_{++} and N^{FG}_{--}) using a normalization factor ($\sqrt{N^{FG}_{++}N^{FG}_{--}}/\sqrt{N^{BG}_{++}N^{BG}_{--}}$). The normalization factor requires that the integrated counts from event mixing equal those from the like-sign in the low mass region

where the correlated pairs are expected to be negligible [39]. The normalized like-sign pairs from event mixing are given as:

$$N^{BG}_{\pm\pm} = \left(N^{BG}_{++} + N^{BG}_{--}\right) \frac{\sqrt{N^{FG}_{++} N^{FG}_{--}}}{\sqrt{N^{BG}_{++} N^{BG}_{--}}}. \quad (2)$$

However, the specific range where the signal of interest is negligible is not well known, and the average of normalization factors over five mass ranges (0.6–2.6 GeV/c^2, 1.0–2.0 GeV/c^2, 1.6–3.2 GeV/c^2, 2.6–3.8 GeV/c^2, and 0.6–4.2 GeV/c^2) is used. The correlated like-sign signal ($N^{\rm cor}_{\pm\pm}$) is then isolated by subtracting the mixed-event spectrum ($N^{BG}_{\pm\pm}$) from the "foreground" like-sign pairs ($N^{FG}_{\pm\pm}$) according to the following,

$$N^{\rm cor}_{\pm\pm} = N^{FG}_{\pm\pm} - N^{BG}_{\pm\pm}. \quad (3)$$

To further improve the normalization process, the $b\bar{b}$ invariant mass distribution shape from PS PYTHIA6 simulation is utilized. This is done by normalizing the integral of the PS PYTHIA6 distribution to the result of Eq. (3), over the signal mass range 5–10 GeV/c^2. The integral of the normalized $b\bar{b}$ mass distribution is then subtracted from the background distribution in Eq. (2) for each of the background ranges and the normalization factor is recalculated. The second step is then repeated until the value of the mixed-events normalization factor converges.

Figure 5 shows the resulting distributions of $N^{FG}_{\pm\pm}$, $N^{BG}_{\pm\pm}$ and $N^{\rm cor}_{\pm\pm}$ as a function of the invariant mass of the pairs. These distributions are corrected with $A\epsilon$. To extract the $b\bar{b}$ distribution as a function of the azimuthal opening angle between muon pairs ($\Delta\phi$) and their p_T, the normalization factors obtained previously are used to normalize $\Delta\phi$ and p_T mixed event distributions, which are then subtracted from $\Delta\phi$ and p_T foreground distributions, respectively.

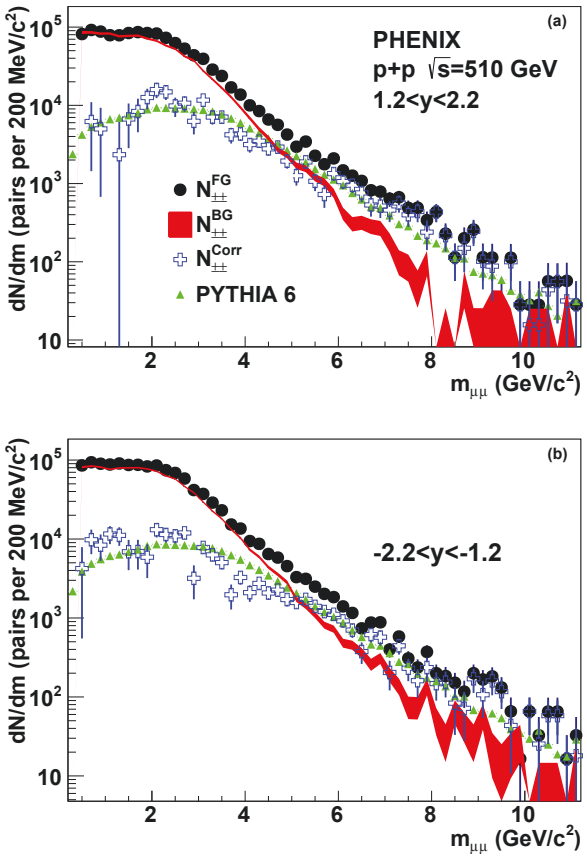

FIG. 5. Invariant mass spectra for like-sign pairs from the same event ($N^{FG}_{\pm\pm}$, solid black points), event-mixing ($N^{BG}_{\pm\pm}$, red band), and the difference between the two ($N^{\rm cor}_{\pm\pm}$, empty blue pluses) for the (a) north arm and (b) south arm. These distributions are corrected with $A\epsilon$. The solid green triangles show PYTHIA $b\bar{b}$ shape.

D. Systematic uncertainties

Table I summarizes the systematic uncertainties. Evaluated as standard deviations, they are divided into three categories based upon the effect each source has on the measured results:

Type-A: Point-to-point uncorrelated uncertainties that allow the data points to move independently with respect to one another and are added in quadrature with statistical uncertainties; however, no systematic uncertainties of this type are associated with this measurement.

Type-B: Point-to-point correlated uncertainties which allow the data points to move coherently within the quoted range to some degree. These systematic uncertainties include a 4% uncertainty from MuID tube efficiency and an 8.2% (2.8%) from MuTr overall efficiency for the north (south) arm. The systematic uncertainty associated with $A\epsilon$ includes the uncertainties on the input p_T and rapidity distributions which are extracted by varying these distributions over the range of the statistical uncertainty of the data, yielding 4.4% (5.0%) for the north (south) arm. To be consistent with the real data analysis, a trigger emulator was used to match the MuIDLL1-2D trigger for the data. The efficiency of the trigger emulator was studied by comparing the dimuon mass spectrum requiring the dimuon passes the trigger emulator to the dimuon mass spectrum requiring the dimuon passes the MuIDLL1-2D trigger, which resulted in a 1.5% (2%) uncertainty for the north (south) arm. Additional 11.2% (8.8%) systematic effect for the north (south) arm was also considered to account for the azimuthal angle distribution difference between data and simulation.

The source of systematic uncertainty in signal ex-

traction is the normalization of mixed events which could come from the choice of the different normalization ranges in the mixed events or $b\bar{b}$ shape from PYTHIA used to guide the signal extraction. A 1.9% uncertainty on the mixed events normalization was observed from using each of the five normalization windows by itself as well as the different combinations of these normalization windows. PYTHIA $b\bar{b}$ shape is the sum of three subprocesses: flavor creation, flavor excitation and gluon splitting. A maximum variation of 3.1% on the extracted signal was observed from choosing each of the subprocesses by itself as the source of $b\bar{b}$ shape. Added in quadrature, they result in a 3.6% uncertainty on signal extraction.

The systematic uncertainty associated with correlated backgrounds could come from the input p_T distribution, differences between GEISHA and FLUKA, and differences between GEANT3 and GEANT4. PYTHIA p_T distributions of $\pi^{\pm}$ and $K^{\pm}$ were compared separately to fits of UA1 data [37, 38] and an overall difference of 18% was observed. Differences of up to 30% and 20% between FLUKA and GEISHA, see Fig. 4, were observed in the north and south arms, respectively. Additional 15% was considered to account for the difference between GEANT3 and GEANT4. Added in quadrature, all three sources give an overall effect on the hadronic background of 39% (31%) for the north (south) arm for the mass and $\Delta\phi$ distributions. For p_T distribution, a p_T-dependent correction was used for the effect on the input p_T spectra and the other two sources gave an overall effect on the hadronic background of 34% (25%) for the north (south) arm. To extract the systematic uncertainty associated with the cross section (or invariant yields) for all distributions (mass, $\Delta\phi$ and p_T), the hadronic background was varied between the limits listed above which resulted in an overall systematic of 5.1% (4.5%) for north (south) arm.

The Type-B systematic uncertainties are added in quadrature and amount to 16.0% (12.8%) for the north (south) arm. They are shown as shaded bands on the associated data points.

Type-C: An overall (global) normalization uncertainty of 10% was assigned for the BBC cross section and efficiency uncertainties [40] which allows the data points to move together by a common multiplicative factor.

TABLE I. Systematic uncertainties associated with the differential cross section calculation in the north (south) arm.

Type	Origin	North (South)
B	MuID hit efficiency	4.0% (4.0%)
B	MuTr hit efficiency	8.2% (2.8%)
B	$A\epsilon$ p_T and y input distributions	4.4% (5.0%)
B	$A\epsilon$ trigger emulator	1.5% (2.0%)
B	$A\epsilon$ ϕ distribution	11.2% (8.8%)
B	Signal extraction	3.6% (3.6%)
B	Correlated background	5.1% (4.5%)
B	Quadratic sum	16.4% (12.8)%
C	MB trigger efficiency	10%

IV. RESULTS AND DISCUSSION

A. Differential cross section

The differential yield and cross section of B meson pairs decaying into like-sign dimuons as a function of mass are calculated according to the following relations,

$$\frac{d^2N}{dydm} = \frac{1}{\Delta y \Delta m}\frac{N_{\mu\mu}}{A\epsilon(y,m)}\frac{\epsilon^{\rm MB}_{\rm BBC}}{\epsilon^{\rm BBC}N_{\rm MB}}\ , \tag{4}$$

$$\frac{d^2\sigma}{dydm} = \frac{d^2N}{dydm}\frac{\sigma^{pp}_{\rm BBC}}{\epsilon^{\rm MB}_{\rm BBC}}\ , \tag{5}$$

where $N_{\mu\mu}/A\epsilon(y,m)$ is the yield of like-sign dimuons from B meson decay normalized by $A\epsilon(y,m)$ in y and m bin with Δy and Δm widths, respectively. The yields of the north and south arms are calculated independently and are consistent within statistical uncertainties; therefore, the weighted average [41] is used in the differential yield calculation. $\sigma^{pp}_{\rm BBC} = 32.5 \pm 3.2$ mb is the cross section as seen for the BBC in p+p collisions at $\sqrt{s} = 510$ GeV, which is determined from the van der Meer scan technique [42]. $\epsilon^{\rm MB}_{\rm BBC} = 0.53 \pm 0.02$ is the fraction of inelastic p+p collisions recorded by the BBC [43]. $\epsilon^{\rm BBC} = 0.91 \pm 0.04$ is the efficiency of the MB trigger for events containing a hard scattering [32]. $N_{\rm MB}$ is the number of MB events.

The differential cross section of like-sign dimuons from B meson decay is shown in Fig. 6. The gray shaded bands represent the weighted average of the quadratic sum of type-B systematic uncertainties of the north and south arms, ≈10.1%. The average is weighted based on the statistical uncertainties of each arm. In addition to type-B systematic uncertainties, we have a 10% global systematic uncertainty for BBC cross section and efficiencies [40].

The total cross section, $d\sigma_{b\bar{b}\to B\bar{B}\to\mu^{\pm}\mu^{\pm}}/dy$, within the mass range, $5 < m_{\mu^{\pm}\mu^{\pm}} < 10$ GeV/c^2, and rapidity and p_T ranges, $1.2 < |y| < 2.2$ and $p_T > 1$ GeV/c, respectively, is extracted

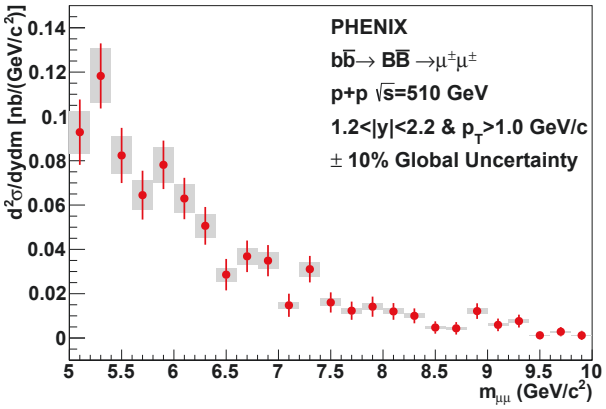

FIG. 6. Differential cross section of like-sign dimuons from B meson decay. The error bars represent the statistical uncertainties, and the gray shaded bands represent the quadratic sum of type-B systematic uncertainties.

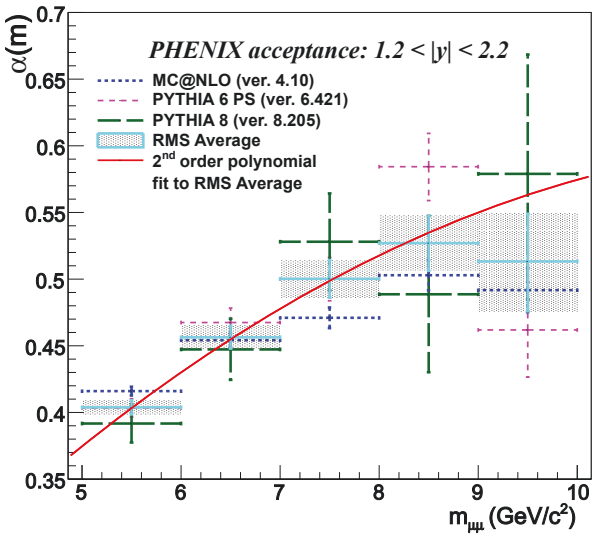

FIG. 7. Fraction of like-sign dimuons from neutral B meson oscillation ($\alpha(m)$) from MC@NLO (blue points) , PS PYTHIA6 (magenta points) and PYTHIA8 (green points) within the PHENIX muon-arms acceptance. Cyan data points are the RMS average of the three model calculations. The shaded boxes are the associated errors based on the three model calculations. The red curve is a second-order polynomial fit to the RMS data points.

by integrating $d^2\sigma_{b\bar{b}\to B\bar{B}\to\mu^\pm\mu^\pm}/dydm$, which resulted $d\sigma_{b\bar{b}\to\mu^\pm\mu^\pm}/dy$ ($1.2 < |y| < 2.2$, $p_T > 1$ GeV/c, $5 < m_{\mu^\pm\mu^\pm} < 10$ GeV/c^2) $= 0.16 \pm 0.01$ (stat) $\pm$ 0.02 (type-B syst) $\pm$ 0.02 (global syst) nb.

To obtain the differential cross section of all B meson pairs that decay into dimuons, regardless of the muon pair charge, the differential cross section of like-sign dimuons from B meson decay is scaled by the ratio of the total number of all B meson pairs that decay into dimuons, regardless of their sign, to those of like-sign. For clarification purposes, the process is divided into two separate steps defined by two variables $\alpha(m)$ and β, both of which depend on the signal from like-sign dimuons due to oscillation.

The ratio of like-sign dimuons at mass m and from primary-primary decays due to B^0 oscillation to like-sign muon pairs resulting from primary-primary or a mixture of primary-secondary decays is defined as:

$$\alpha(m) = \frac{b\bar{b} \to B\bar{B} \to \mu^\pm\mu^\pm \text{ (osc)}}{b\bar{b} \to B\bar{B} \to \mu^\pm\mu^\pm}, \qquad (6)$$

which is calculated in the mass range $5 < m < 10$ GeV/c^2 at $1.2 < |y| < 2.2$ and $p_T > 1$ GeV/c and extrapolates the correlated like-sign signal to an open bottom signal from oscillation, $N^{osc}_{\pm\pm}$. The $\alpha(m)$ is obtained using open bottom events from three model calculations: MC@NLO (ver 4.10), PS PYTHIA6 (ver 6.421) and PYTHIA8 (ver 8.205) as shown in Fig. 7. The red line is a second-order polynomial fit with χ^2/ndf of 3.8/4. The shaded boxes represent the uncertainty based on the three model calculations.

β is the ratio of primary-primary like-sign dimuons due to B^0 oscillation to all B meson pairs that decay into primary-primary dimuons with all possible muon charge pairs ($++$, $--$ and $+-$). β converts the number of muon pairs from oscillation into all B meson pairs and is defined as:

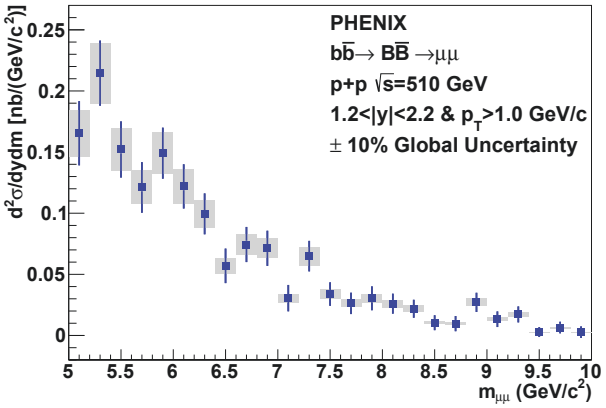

FIG. 8. Differential cross section of all dimuons from B meson decay. The error bars represent the statistical uncertainties, and the gray shaded band represents the quadratic sum of type-B systematic uncertainties.

$$\beta = \frac{b\bar{b} \to B\bar{B} \to \mu^\pm\mu^\pm \text{ (osc)}}{b\bar{b} \to B\bar{B} \to \mu\mu}. \qquad (7)$$

The value of β is 0.22 ± 0.01 which is the calculated RMS value from the three model simulations described above. The error of β is the standard deviation of the three model calculations which represents the model-dependent uncertainty.

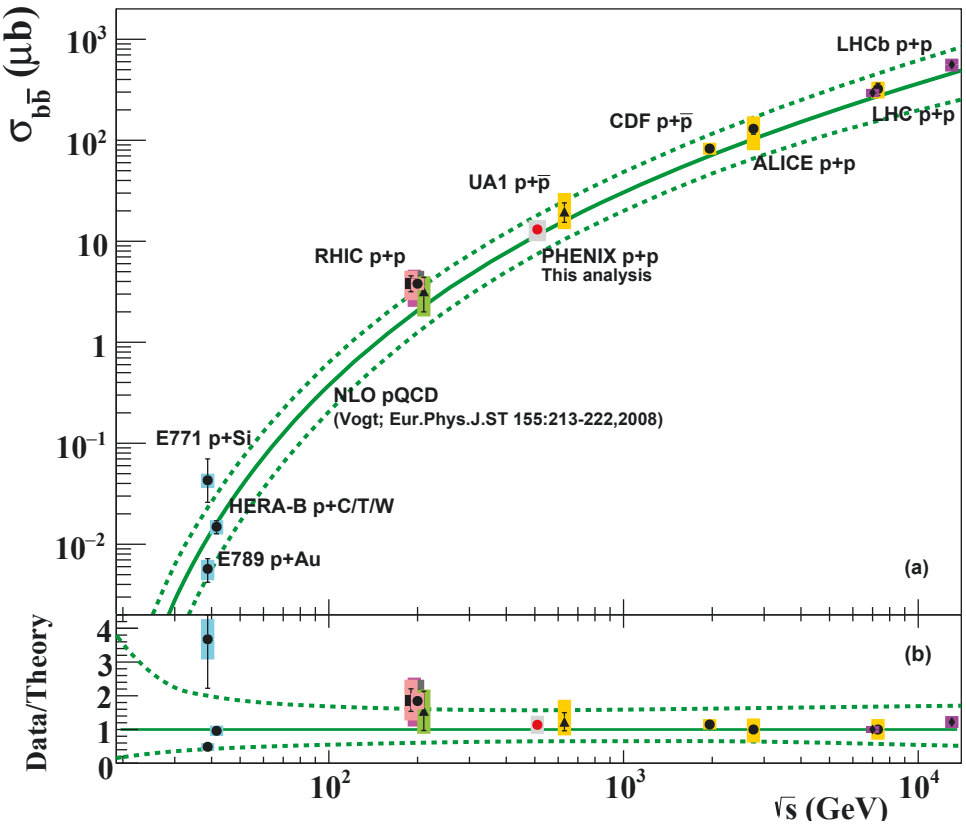

FIG. 9. (a) Bottom cross section, $\sigma_{b\bar{b}}$ as a function of $\sqrt{s}$. The curves are NLO pQCD calculation [44] with the dashed lines being error bands obtained by varying the renormalization scale, factorization scale and bottom quark mass. (b) Ratio of data to NLO pQCD calculation.

The differential cross section of all B meson pairs that decay into a primary-primary dimuon, regardless of the muon pair charge, is then calculated as follows:

$$\frac{d^2\sigma_{b\bar{b}\to B\bar{B}\to\mu\mu}}{dydm} = \frac{\alpha(m)}{\beta}\frac{d^2\sigma_{b\bar{b}\to B\bar{B}\to\mu^\pm\mu^\pm}}{dydm}. \quad (8)$$

Figure 8 shows the differential cross section of all B meson pairs that decay into a primary-primary dimuon. Additional type-B systematic uncertainties associated with this measurement due to $\alpha(m)$ and β and amount to 1.9% and 4.5%, respectively, are included. This brings the type-B systematic uncertainties on $d^2\sigma_{b\bar{b}\to B\bar{B}\to\mu\mu}/dydm$ to 11.2%.

The total cross section, $d\sigma_{b\bar{b}\to B\bar{B}\to\mu\mu}/dy$, within the mass range, $5.0 < m_{\mu\mu} < 10.$ GeV/c^2, and rapidity and p_T ranges, $1.2 < |y| < 2.2$ and $p_T > 1$ GeV/c, respectively, is extracted by integrating $d^2\sigma_{b\bar{b}\to B\bar{B}\to\mu\mu}/dydm$, which resulted $d\sigma_{b\bar{b}\to\mu\mu}/dy$ ($1.2 < |y| < 2.2$, $p_T > 1$ GeV/c, $5 < m_{\mu\mu} < 10$ GeV/c^2) $= 0.31 \pm 0.01$ (stat) $\pm$ 0.04 (type-B syst) $\pm$ 0.03 (global syst) nb.

B. Total cross section

To extrapolate from the $b\bar{b}$ differential cross section in the muon decay channel within the acceptance of muon arms to a total $b\bar{b}$ cross section, the differential cross section is scaled by the ratio of B pairs that decay to dimuons within the measured region to those over the entire kinematic range. This method is similar to that found in Ref. [45].

The total cross section, $\sigma_{b\bar{b}}$, is extrapolated and corrected for the semileptonic branching ratio in the following manner:

$$\sigma_{b\bar{b}} = \frac{d\sigma_{b\bar{b}\to\mu\mu}}{dy} \times \frac{1}{scale} \times \frac{1}{(BR_{B\to\mu})^2}\,, \quad (9)$$

where $BR_{B\to\mu}$ is the branching ratio of B to muon through the primary decay channel (=10.99%), and *scale*, defined as:

$$scale = \frac{B\bar{B}\to\mu\mu(1.2<y<2.2; p_T>1; 5<m_{\mu\mu}<10)}{B\bar{B}\to\mu\mu(all)}, \quad (10)$$

which is a factor used to convert from the visible kinematic region to full phase space. The *scale* factor is determined from PYTHIA and MC@NLO simulations. It is taken as the average value, 1.96×10^{-3}, of PS PYTHIA6 (CTEQ6LL), PS PYTHIA6 (CTEQ5M1), PYTHIA8 (CTEQ6LL) and MC@NLO (CTEQ5M) as listed in Table II.

The difference in the *scale* factor due to the different models and parton distribution functions is considered to be a global type-C uncertainty, which amounts to 18.1%. This results in a total cross section of 13.1 $\pm$

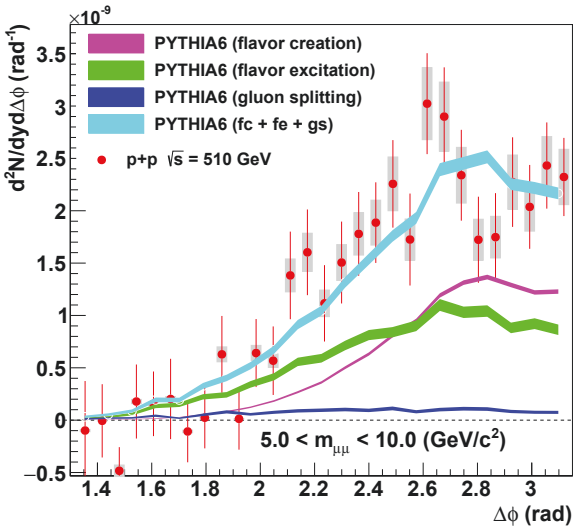

FIG. 10. Like-sign $\mu\mu$ yield as a function of the azimuthal opening angle. The data are compared to the distributions calculated with PS PYTHIA6. The model calculations are normalized to the data. For PS PYTHIA6 the $\mu\mu$ pair yield is broken down into contributions from flavor creation, flavor excitation, and gluon splitting.

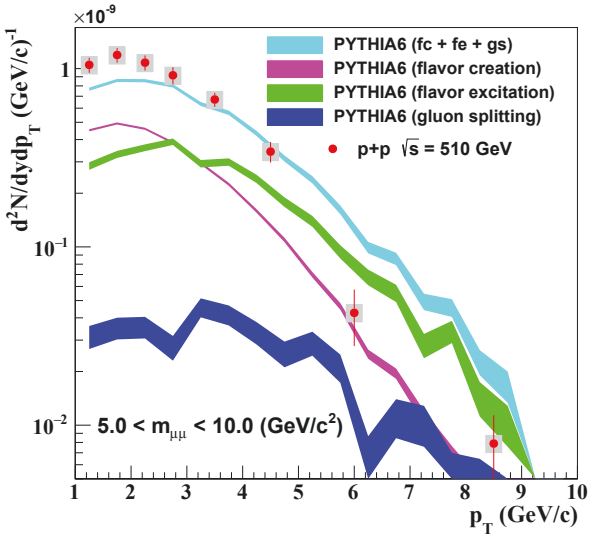

FIG. 11. Like-sign $\mu\mu$ yield as a function of the pair p_T. The data are compared to the distributions calculated with PS PYTHIA6. The model calculations are normalized to the data. For PS PYTHIA6 the $\mu\mu$ pair yield is broken down into contributions from flavor creation, flavor excitation, and gluon splitting.

TABLE II. Values of the scale factor as found using PS PYTHIA6 [26], PYTHIA8 [27], and MC@NLO [28].

Simulation	Scale Factor
PYTHIA8 (CTEQ6LL)	0.00210
PS PYTHIA6 (CTEQ6LL)	0.00207
PS PYTHIA6 (CTEQ5M1)	0.00255
MC@NLO (CTEQ5M)	0.00113
Average Value	0.00196

0.6 (stat)±1.5 (type-B syst)±2.7 (global syst) μb. Type-B systematic uncertainties are from the differential cross section while global uncertainties are the quadrature sum of type-C from the differential cross section and uncertainties arising from the extrapolation.

The $\sigma_{b\bar{b}}$ measured at $\sqrt{s}$ = 510 GeV is shown in Fig. 9 and compared to measurements from other experiments [2–4, 9, 17, 46]. The solid line is the cross section from NLO pQCD calculations [44] and the dashed lines are error bands, and they are obtained by varying the renormalization scale, factorization scale and bottom quark mass. At $\sqrt{s}$ = 510 GeV, the NLO pQCD calculation predicts $\sigma_{b\bar{b}} = 11.5^{+6.5}_{-3.9}$ μb, which is consistent with the extrapolated total cross section using the current dimuon analysis within uncertainties. Figure 9 also shows the ratio of data to theory.

C. Azimuthal correlations and pair p_T

The like-sign $\mu\mu$ pair yield from $b\bar{b}$ decays is shown in Fig. 10 and Fig. 11 as a function of $\Delta\phi$ and pair p_T, respectively. The spectra are compared to model calculations based on PS PYTHIA6 that are normalized by fitting the subprocesses sum to the data [18]. The generated pairs are filtered with the same kinematic cuts that are applied in the data analysis.

The azimuthal opening angle distribution from PS PYTHIA6 shows a similar pattern to that of the data, an increase until ≈2.6 rad and then drop, and it is consistent with the data with χ^2/ndf≈27/28, when considering the quadrature sum of the statistical and systematic uncertainties. The data show steeper p_T dependence than that of PS PYTHIA6 but they are still consistent when considering the large statistical and systematic uncertainties. We note that flavor creation fits the data much better than any other subprocess with χ^2/ndf≈8.4/7. These results show similar behavior to that observed at 200 GeV [18] where the data favors a dominant mix of flavor creation and flavor excitation subprocesses over gluon splitting.

V. SUMMARY AND CONCLUSION

In summary, we presented first measurements of the differential cross section for dimuons from bottom quark-antiquark production in p+p collisions at $\sqrt{s}$ = 510 GeV, which we found to be: $d\sigma_{b\bar{b}\to\mu^\pm\mu^\pm}/dy = 0.16 \pm 0.01$ (stat) $\pm$ 0.02 (syst) $\pm$ 0.02 (global) nb. The analysis

technique is based on the yield of high-mass correlated like-sign dimuons from parity-violating decays of B meson pairs at forward and backward rapidities. Using a model dependent extrapolation, the measured differential cross section is converted to a total cross section of 13.1±0.6 (stat)±1.5 (syst)±2.7 (global) μb. This extrapolated total cross section is consistent with NLO pQCD calculations within uncertainties. This agreement with NLO pQCD calculations at $\sqrt{s} = 510$ GeV is better than what was observed at 200 GeV [18], possibly indicating a better match with NLO pQCD calculations at higher energies. However, the measurement at $\sqrt{s} = 200$ GeV used the unlike-sign pairs method and could be impacted by the presence of Drell-Yan process and resonances.

The azimuthal opening angle between the muons from $b\bar{b}$ decays and the pair p_T distributions are compared to distributions generated using PS PYTHIA6 [26], which includes NLO processes. While the data tend to have a wider azimuthal distribution than PS PYTHIA6 calculations and present a steeper p_T distribution, both are still consistent within uncertainties with PS PYTHIA6, where flavor creation and flavor excitation subprocesses are dominant. This is similar to what was observed at 200 GeV [18].

ACKNOWLEDGMENTS

We thank the staff of the Collider-Accelerator and Physics Departments at Brookhaven National Laboratory and the staff of the other PHENIX participating institutions for their vital contributions. We acknowledge support from the Office of Nuclear Physics in the Office of Science of the Department of Energy, the National Science Foundation, Abilene Christian University Research Council, Research Foundation of SUNY, and Dean of the College of Arts and Sciences, Vanderbilt University (U.S.A), Ministry of Education, Culture, Sports, Science, and Technology and the Japan Society for the Promotion of Science (Japan), Conselho Nacional de Desenvolvimento Científico e Tecnológico and Fundação de Amparo à Pesquisa do Estado de São Paulo (Brazil), Natural Science Foundation of China (People's Republic of China), Croatian Science Foundation and Ministry of Science and Education (Croatia), Ministry of Education, Youth and Sports (Czech Republic), Centre National de la Recherche Scientifique, Commissariat à l'Énergie Atomique, and Institut National de Physique Nucléaire et de Physique des Particules (France), Bundesministerium für Bildung und Forschung, Deutscher Akademischer Austausch Dienst, and Alexander von Humboldt Stiftung (Germany), J. Bolyai Research Scholarship, EFOP, the New National Excellence Program (ÚNKP), NKFIH, and OTKA (Hungary), Department of Atomic Energy and Department of Science and Technology (India), Israel Science Foundation (Israel), Basic Science Research and SRC(CENuM) Programs through NRF funded by the Ministry of Education and the Ministry of Science and ICT (Korea). Physics Department, Lahore University of Management Sciences (Pakistan), Ministry of Education and Science, Russian Academy of Sciences, Federal Agency of Atomic Energy (Russia), VR and Wallenberg Foundation (Sweden), the U.S. Civilian Research and Development Foundation for the Independent States of the Former Soviet Union, the Hungarian American Enterprise Scholarship Fund, the US-Hungarian Fulbright Foundation, and the US-Israel Binational Science Foundation.

[1] M. L. Mangano, P. Nason, and G. Ridolfi, "Heavy-quark correlations in hadron collisions at next-to-leading order," Nucl. Phys. B **373**, 295 (1992).

[2] T. Alexopoulos *et al.* (E771 Collaboration), "Measurement of the $b\bar{b}$ Cross Section in 800 GeV/c Proton-Silicon Interactions," Phys. Rev. Lett. **82**, 41 (1999).

[3] D. M. Jansen *et al.*, "Measurement of the Bottom-Quark Production Cross Section in 800 GeV/c Proton-Gold Collisions," Phys. Rev. Lett. **74**, 3118 (1995).

[4] I. Abt *et al.* (HERA-B Collaboration), "Improved measurement of the $b\bar{b}$ production cross section in 920 GeV fixed-target proton-nucleus collisions," Phys. Rev. D **73**, 052005 (2006).

[5] D. Acosta *et al.* (CDF Collaboration), "Measurement of the J/ψ meson and b-hadron production cross sections in $p\bar{p}$ collisions at $\sqrt{s} = 1960$ GeV," Phys. Rev. D **71**, 032001 (2005).

[6] R. Aaij *et al.* (LHCb Collaboration), "Measurement of $\sigma(pp \to b\bar{b}X)$ at $\sqrt{s} = 7$ TeV in the forward region," Phys. Lett. B **694**, 209 (2010).

[7] R Aaij *et al.* (LHCb Collaboration), "Measurement of B meson production cross-sections in proton-proton collisions at $\sqrt{s} = 7$ TeV", J. High Energy Phys. 08 (2013), 117.

[8] G. Aad *et al.* (ATLAS Collaboration), "Measurement of the b-hadron production cross section using decays to $D^*\mu^- X$ final states in pp collisions at $\sqrt{(}s) = 7$ TeV with the ATLAS detector," Nucl. Phys. B **864**, 341 (2012).

[9] B. Abelev *et al.* (ALICE Collaboration), "Measurement of electrons from beauty hadron decays in pp collisions at $\sqrt{s} = 7$ TeV," Phys. Lett. B **721**, 13 (2013).

[10] V. Khachatryan *et al.* (CMS Collaboration), "Measurement of the B^+ Production Cross Section in pp Collisions at $\sqrt{s} = 7$ TeV," Phys. Rev. Lett. **106**, 112001 (2011).

[11] S. Chatrchyan *et al.* (CMS Collaboration), "Measurement of the B^0 Production Cross Section in pp Collisions at $\sqrt{s} = 7$ TeV," Phys. Rev. Lett. **106**, 252001 (2011).

[12] S. Chatrchyan *et al.* (CMS Collaboration), "Measurement of the cross section for production of $b\bar{b}\,X$, decaying to muons in pp collisions at $\sqrt{s} = 7$ TeV", J. High Energy Phys. 06 (2012), 110.

[13] A. Adare *et al.* (PHENIX Collaboration), "Cross section for $b\bar{b}$ production via dielectrons in d+Au collisions at $\sqrt{s_{NN}} = 200$ GeV," Phys. Rev. C **91**, 014907 (2015).

[14] A. Adare *et al.* (PHENIX Collaboration), "Measurement of Bottom Versus Charm as a Function of Transverse Momentum with Electron-Hadron Correlations in $p+p$ Collisions at $\sqrt{s} = 200$ GeV," Phys. Rev. Lett. **103**, 082002 (2009).

[15] M. M. Aggarwal *et al.* (STAR Collaboration), "Measurement of the Bottom contribution to non-photonic electron production in $p + p$ collisions at $\sqrt{s} = 200$ GeV," Phys. Rev. Lett. **105**, 202301 (2010).

[16] C. Aidala *et al.* (PHENIX Collaboration), "B-meson production at forward and backward rapidity in $p + p$ and Cu + Au collisions at $\sqrt{s_{NN}} = 200$ GeV," Phys. Rev. C **96**, 064901 (2017).

[17] A. Adare *et al.* (PHENIX Collaboration), "Dilepton mass spectra in $p + p$ collisions at $\sqrt{s} = 200$ GeV and the contribution from open charm," Phys. Lett. B **670**, 313 (2009).

[18] C. Aidala *et al.* (PHENIX Collaboration), "Measurements of $\mu\mu$ pairs from open heavy flavor and Drell-Yan in $p + p$ collisions at $\sqrt{s} = 200$ GeV," Phys. Rev. D **99**, 072003 (2019).

[19] A. Bean *et al.* (CLEO Collaboration), "Limits on $B^0\bar{B}^0$ Mixing and τ_{B^0}/τ_{B^+}," Phys. Rev. Lett. **58**, 183 (1987).

[20] H. Albrecht *et al.* (ARGUS Collaboration), "Observation of B^0-$\bar{B}^0$ Mixing," Phys. Lett. B **192**, 245 (1987).

[21] D. Buskulic *et al.* (ALEPHI Collaboration), "An investigation of B_d^0 and B_s^0 oscillation," Phys. Lett. B **322**, 441 (1994).

[22] C. Albajar *et al.* (UA1 Collaboration), "Search for B^0-$\bar{B}^0$ oscillations at the CERN proton- antiproton collider," Phys. Lett. B **186**, 247 (1987), [Erratum: Phys. Lett. B **197**, 565 (1987)].

[23] S. L. Glashow, "Partial Symmetries of Weak Interactions," Nucl. Phys. **22**, 579 (1961).

[24] F. Abe *et al.* (CDF Collaboration), "Measurement of $B^0\overline{B}^0$ flavor oscillations using jet-charge and lepton flavor tagging in $p\bar{p}$ collisions at $\sqrt{s} = 1.8$ TeV," Phys. Rev. D **60**, 072003 (1999).

[25] K. A. Olive *et al.* (Particle Data Group), "Review of Particle Physics," Chin. Phys. C **38**, 090001 (2014).

[26] T. Sjostrand, P. Eden, C. Friberg, L. Lonnblad, G. Miu, S. Mrenna, and E. Norrbin, "High-energy-physics event generation with PYTHIA 6.1," Comp. Phys. Commun. **135**, 238 (2001).

[27] T. Sjöbstrand, S. Ask, J. R. Christiansen, R. Corke, N. Desai, P. Ilten, S. Mrenna, S. Stefan Prestel, C. O. Rasmussen, and P. Z. Skands, "An introduction to PYTHIA8.2," Comp. Phys. Commun. **191**, 159 (2015).

[28] S. Frixione and B. R. Webber, "Matching NLO QCD Computations and Parton Shower Simulations", J. High Energy Phys. 06 (2002), 029.

[29] K. Adcox *et al.* (PHENIX Collaboration), "PHENIX detector overview," Nucl. Instrum. Methods Phys. Res., Sec. A **499**, 469 (2003).

[30] R. Field and R. C. Group (CDF Collaboration), "PYTHIA Tune A, HERWIG, and JIMMY in Run 2 at CDF", arXiv:hep-ph/0510198 (2005).

[31] S. Agostinelli *et al.*, "GEANT4 a simulation toolkit," Nucl. Instrum. Methods Phys. Res., Sec. A **506**, 250 (2003).

[32] U. A. Acharya *et al.* (PHENIX Collaboration), "J/ψ and $\psi(2S)$ production at forward rapidity in p+p collisions at $\sqrt{s} = 510$ GeV," Phys. Rev. D **101**, 052006 (2020).

[33] R. Aaij *et al.* (LHCb Collaboration), "Observation of D^0-$\bar{D}^0$ oscillations," Phys. Rev. Lett. **110**, 101802 (2013).

[34] A. Adare *et al.* (PHENIX Collaboration), "Event structure and double helicity asymmetry in jet production from polarized $p + p$ collisions at $\sqrt{s} = 200$ GeV," Phys. Rev. D **84**, 012006 (2011).

[35] R. Brun, F. Carminati, and S. Giani, "GEANT Detector Description and Simulation Tool", CERN-W-5013 (1994).

[36] A. Adare *et al.* (PHENIX Collaboration), "Nuclear-modification factor for open-heavy-flavor production at forward rapidity in Cu+Cu collisions at $\sqrt{s_{NN}} = 200$ GeV," Phys. Rev. C **86**, 024909 (2012).

[37] A. Adare *et al.* (PHENIX Collaboration), "Cross section and longitudinal single-spin asymmetry A_L for forward $W^\pm \to \mu^\pm\nu$ production in polarized $p + p$ collisions at $\sqrt{s} = 510$ GeV," Phys. Rev. D **98**, 032007 (2018).

[38] C. Albajar *et al.*, "A study of the general characteristics of proton-antiproton collisions at $\sqrt{s} = 0.2$ to 0.9 TeV," Nucl. Phys. B **335**, 261 (1990).

[39] P. Crochet and P. Braun-Munzinger, "Investigation of background subtraction techniques for high mass dilepton physics," Nucl. Instrum. Methods Phys. Res., Sec. A **484**, 564 (2002).

[40] S. S. Adler *et al.* (PHENIX Collaboration), "Midrapidity Neutral-Pion Production in Proton-Proton Collisions at $\sqrt{s} = 200$ GeV," Phys. Rev. Lett. **91**, 241803 (2003).

[41] R. Nisius, "On the combination of correlated estimates of a physics observable," Eur. Phys. J. C **74**, 3004 (2014).

[42] A. Adare *et al.* (PHENIX Collaboration), "Cross Section and Parity-Violating Spin Asymmetries of $W^\pm$ Boson Production in Polarized $p + p$ Collisions at $\sqrt{s} = 500$ GeV," Phys. Rev. Lett. **106**, 062001 (2011).

[43] A. Adare *et al.* (PHENIX Collaboration), "Inclusive cross section and double helicity asymmetry for π^0 production in $p + p$ collisions at $\sqrt{s} = 62.4$ GeV," Phys. Rev. D **79**, 012003 (2009).

[44] R. Vogt, "The total charm cross-section," Eur. Phys. J. Special Topics **155**, 213 (2008).

[45] Chekanov S. *et al.* (ZEUS Collaboration), "Measurement of beauty production from dimuon events at HERA", J. High Energy Phys. 02 (2009), 032.

[46] C. Albajar *et al.* (UA1 Collaboration), "Beauty production at the CERN $p\bar{p}$ collider," Phys. Lett. B **256**, 121 (1991).